AIP Advances

The 3D-tomography of the nano-clusters formed by Fe-coating and annealing of diamond films for enhancing their surface electron field emitters

Huang-Chin Chen, Shen-Chuan Lo, Li-Jiaun Lin, Pin-Chang Huang, Wen-Ching Shih, I-Nan Lin, and Chi-Young Lee

Citation: AIP Advances **2**, 032153 (2012); doi: 10.1063/1.4748865
View online: http://dx.doi.org/10.1063/1.4748865
View Table of Contents: http://scitation.aip.org/content/aip/journal/adva/2/3?ver=pdfcov
Published by the AIP Publishing

Articles you may be interested in

The microstructural evolution of ultrananocrystalline diamond films due to P ion implantation process—the annealing effect
J. Appl. Phys. **116**, 183701 (2014); 10.1063/1.4901333

Enhancing electrical conductivity and electron field emission properties of ultrananocrystalline diamond films by copper ion implantation and annealing
J. Appl. Phys. **115**, 063701 (2014); 10.1063/1.4865325

The induction of nanographitic phase on Fe coated diamond films for the enhancement in electron field emission properties
J. Appl. Phys. **113**, 094305 (2013); 10.1063/1.4792520

Modification of ultrananocrystalline diamond film microstructure via Fe-coating and annealing for enhancement of electron field emission properties
J. Appl. Phys. **112**, 033708 (2012); 10.1063/1.4739772

The induction of a graphite-like phase on diamond films by a Fe-coating/post-annealing process to improve their electron field emission properties
J. Appl. Phys. **109**, 084309 (2011); 10.1063/1.3569887

All article content, except where otherwise noted, is licensed under a Creative Commons Attribution 3.0 Unported license. See: http://creativecommons.org/licenses/by/3.0/
Downloaded to IP: 163.13.36.187 On: Tue, 14 Apr 2015 07:05:07

The 3D-tomography of the nano-clusters formed by Fe-coating and annealing of diamond films for enhancing their surface electron field emitters

Huang-Chin Chen,[1,4] Shen-Chuan Lo,[2] Li-Jiaun Lin,[2] Pin-Chang Huang,[3] Wen-Ching Shih,[3] I-Nan Lin,[1,a] and Chi-Young Lee[4,a]

[1]*Department of Physics, Tamkang University, New-Taipei 251, Taiwan, Republic of China*
[2]*Department of Microstructure and Characterization, Material and Chemical Research Laboratories, Industrial Technology Research Institute, Hsin-Chu 310, Taiwan, Republic of China*
[3]*Graduate Institute in Electro-Optical Engineering, Tatung University, Taipei 104, Taiwan, Republic of China*
[4]*Department of Materials Science and Engineering, National Tsing-Hua University, Hsinchu 300, Taiwan, Republic of China*

(Received 14 May 2012; accepted 14 August 2012; published online 23 August 2012)

The Fe-coating and H_2-annealed processes markedly increased the conductivity and enhanced the surface electron field emission (s-EFE) properties for the diamond films. The enhancement on the s-EFE properties for the diamond films is presumably owing to the formation of nano-graphite clusters on the surface of the films via the Fe-to-diamond interaction. However, the extent of enhancement varied with the granular structure of the diamond films. For the microcrystalline (MCD) films, the s-EFE process can be turned on at $(E_0)_{MCD} = 1.9$ V/μm, achieving a large s-EFE current density of $(J_e)_{MCD} = 315$ μA/cm^2 at an applied field of 8.8 V/μm. These s-EFE properties are markedly better than those for Fe-coated/annealed ultrananocrystalline diamond (UNCD) films with $(E_0)_{UNCD} = 2.0$ V/μm and $(J_e)_{UNCD} = 120$ μA/cm^2. The transmission electron microscopy showed that the nano-graphite clusters formed an interconnected network for MCD films that facilitated the electron transport more markedly, as compared with the isolated nano-graphitic clusters formed at the surface of the UNCD films. Therefore, the Fe-coating/annealing processes improved the s-EFE properties for the MCD films more markedly than that for the UNCD films. The understanding on the distribution of the nano-clusters is of critical importance in elucidating the authentic factor that influences the s-EFE properties of the diamond films. Such an understanding is possible only through the 3D-tomographic investigations. *Copyright 2012 Author(s). This article is distributed under a Creative Commons Attribution 3.0 Unported License*. [http://dx.doi.org/10.1063/1.4748865]

I. INTRODUCTION

Diamond films possess many desirable physical and chemical properties[1–3] and have been the focus of intensive research since the successful synthesis of diamond in microwave plasma enhanced chemical vapour deposition (CVD) process.[4] Diamond films have been extensively investigated for their application as electron field emitters due to their negative electron affinity (NEA) properties.[5] Generally, a good electron field emitter requires sufficient supply of electrons from the back contact materials, effective transport of electrons through the films and efficient emission from the emitting sites. The large electronic band gap (5.5 eV) of diamond films hinder tremendously the electron field emission (EFE) behaviour due to lack of free electrons required for field emission. The unavailability of highly conducting diamond limits use of this material in EFE devices. Addition of p-type

[a]Corresponding author: CY Lee (e-mail: cylee@mx.nthu.edu.tw) and IN Lin (inanlin@mail.tku.edu.tw)

 © Author(s) 2012

All article content, except where otherwise noted, is licensed under a Creative Commons Attribution 3.0 Unported license. See: http://creativecommons.org/licenses/by/3.0/
Downloaded to IP: 163.13.36.187 On: Tue, 14 Apr 2015 07:05:07

(eg. boron) or n-type (eg. phosphorus, sulphur etc.) dopants can render MCD diamond conductive. Diverse reports on B, P and S doped diamond highlight the effect of various film deposition conditions and structural evolution which facilitates in defining properties of the films.[6–16] On the other hand, ultrananocrystalline diamond (UNCD) films possess smoother surface and better conductivity than the conventional microscrystallilne diamond (MCD) films and are advantageous in device application.[17,18] However, for UNCD films, the conventional dopants, B, P and S do not effectively improve their conductivity. Nitrogen is known to be a good source for n-type doping for UNCD films.[19] The N_2 incorporation on improving the structural properties, electrical conductivity, electron field emission (EFE) properties of doped UNCD films have been demonstrated.[19–24] However, the EFE properties of these materials are still not satisfactory due to the insufficient conductivity for the diamond films. Transporting the electrons across the surface of the diamond films, instead of conducting them through the diamond films, before being field emitted, resulting in a surface electron emitters (s-EFE) process, is another feasible approach for synthesizing an electron field emitter. Previous studies,[25,26] we observed an improved s-EFE properties of diamond by Fe-coating/annealing processes. However, the extent of improvement differed markedly for the MCD and UNCD films. The genuine factor is still not completely understood.

In this paper, we investigated the evolution of microstructure of MCD and UNCD films due to these Fe-coating/annealing processes by using a high angle annular dark field (HAADF) and a 3D-tomography technique in transmission electron microscopy. The mechanism for the different enhancement on the s-EFE process by these Fe-coating/annealing processes due to the difference in granular structure of the diamond films was discussed based on these observations.

II. EXPERIMENTAL

Diamond films were grown on p-type silicon substrates in microwave plasma enhanced chemical vapour deposition (IPLAS-Cyrannus) system. The substrates were first thoroughly cleaned by rinsed the Si wafer sequentially in water-diluted hydrogen peroxide/ammonium hydroxide and hydrogen peroxide/hydrochloric acid solution. Then the substrates were ultrasonicated in a solution containing nanodiamond and titanium powders for 45 min to facilitate the nucleation of diamond, followed by ultrasonication in methanol solution to remove the possibly adhered diamond and Ti nano-particles. The microcrystalline diamond (MCD) films were grown in CH_4/H_2 = 1/99 sccm plasma excited by a 1400 W (2.45 GHz) microwave with 55 torr total pressure, whereas the ultrananocrystalline diamond (UNCD) films were grown in CH_4/Ar = 2/98 sccm plasma excited by a 1400 W microwave with 120 torr total pressure, for 1 h. The diamond films were coated with a thin layer of iron by DC sputtering process for 1 min to a thickness around 10 nm. They were then thermally post-annealed at 900°C in H_2 atmosphere, with a flow rate of 100 sccm for 5 min. The heating and cooling rate are around 15 °C/min.

The morphology and structure of the films were investigated, respectively, by field emission scanning electron microscope (FESEM, CARL ZEISS, SUPRA 55) and the Raman spectroscopy (Renishaw, Model-INVIA) with a back scattering geometry using 514.5 nm line of an Ar-ion laser. The field emission measurements were carried out by a tunable parallel plate setup. The separation of the anode (Mo) tip from the sample was controlled using a digital micrometer that was monitored by an optical microscope. Notably, in the measuring of the EFE properties, the Cu-foil attached to the bottom of Si-substrate was wrapped over to contact the surface of the diamond films such that the electrons were transported along the surface of the films, rather than from bottom through the films to the top surface, before being field emitted. The J-E curves thus measured actually represent the "surface electron field emission (s-EFE) behavior", instead of the "through films EFE behavior", of the MCD and UNCD films. The s-EFE properties of the samples were analyzed by using the Fowler–Nordheim (F-N) model.[27]

$$\mathrm{J(E)} = \mathrm{AE}^2 \exp\left[\frac{-\mathrm{B}\phi^{3/2}}{E}\right],$$

$$\text{with} \quad A = e^3/16\pi^2 h\phi t^2(y_0) \quad \text{and} \quad B = 4/3e\,(2m/h^2)^{1/2} v(y_0)$$

All article content, except where otherwise noted, is licensed under a Creative Commons Attribution 3.0 Unported license. See: http://creativecommons.org/licenses/by/3.0/
Downloaded to IP: 163.13.36.187 On: Tue, 14 Apr 2015 07:05:07

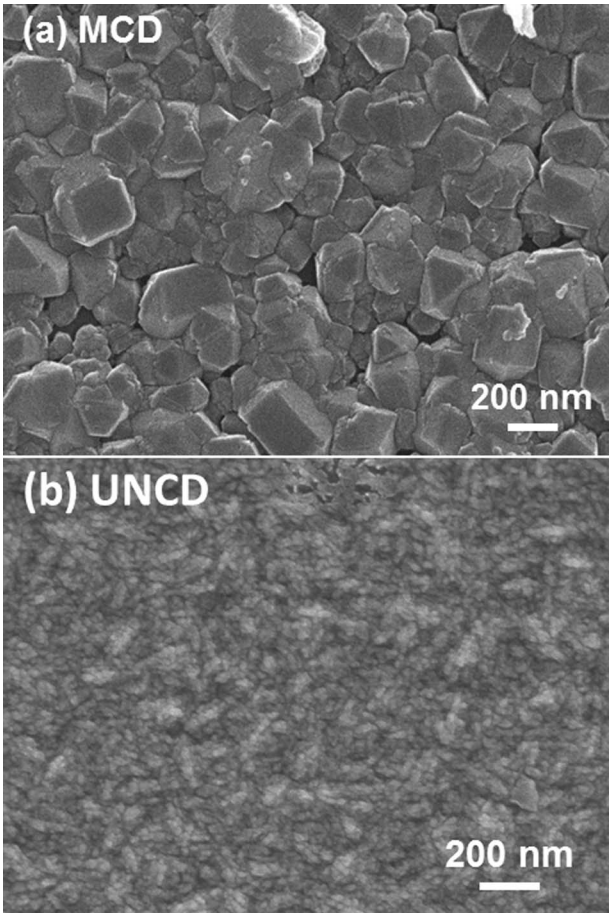

FIG. 1. The SEM micrograph of the as-grown (a) MCD and (b) UNCD films.

where φ is the work function of the emission materials. The J & E are EFE current density and applied field, respectively. The turn-on field was designated as the interception of the lines extrapolated from the high-field and low-field segments of F-N plots.

The detailed microstructure was examined using high resolution transmission electron microscopy (HRTEM, Joel 2100) and the distribution of the Fe-, Fe_3C- and nanographite-clusters were investigated by a high angle annular dark field (HAADF) and a 3D-tomography in TEM. Notably, in TEM, when the elastically scattered electrons were diffracted coherently, diffraction contrast image will be resulted that provides the structure information of the samples. Moreover, some of the elastically scattered electrons were incoherent. The scattering angle is closely related to the atomic number of the species involved. The heavier the species are, the larger the scattering angle. When the incoherently scattered electrons were collected by a high angle annular detector, a HAADF image[28–30] will be obtained. The HAADF-image provides the information on the elemental distribution on the samples. The 3D-tomography is the HAADF images taken with the samples tilted stepwisely (2°) and was then replayed sequentially using a software *Digital-Micrograph (Joel)*.[31]

III. RESULTS

The characteristics of MCD films are markedly different from those of UNCD films owing to the difference in granular structure of the two films. Figures 1(a) and 1(b) show the SEM morphology of the as-deposited MCD and UNCD films, respectively. The MCD films contain large grains (∼∼200–400 nm) with faceted geometry, whereas the UNCD films contain ultra-small grains (∼5 nm) with equi-axed geometry. The Raman spectroscopy of the MCD films shows prominent

All article content, except where otherwise noted, is licensed under a Creative Commons Attribution 3.0 Unported license. See: http://creativecommons.org/licenses/by/3.0/
Downloaded to IP: 163.13.36.187 On: Tue, 14 Apr 2015 07:05:07

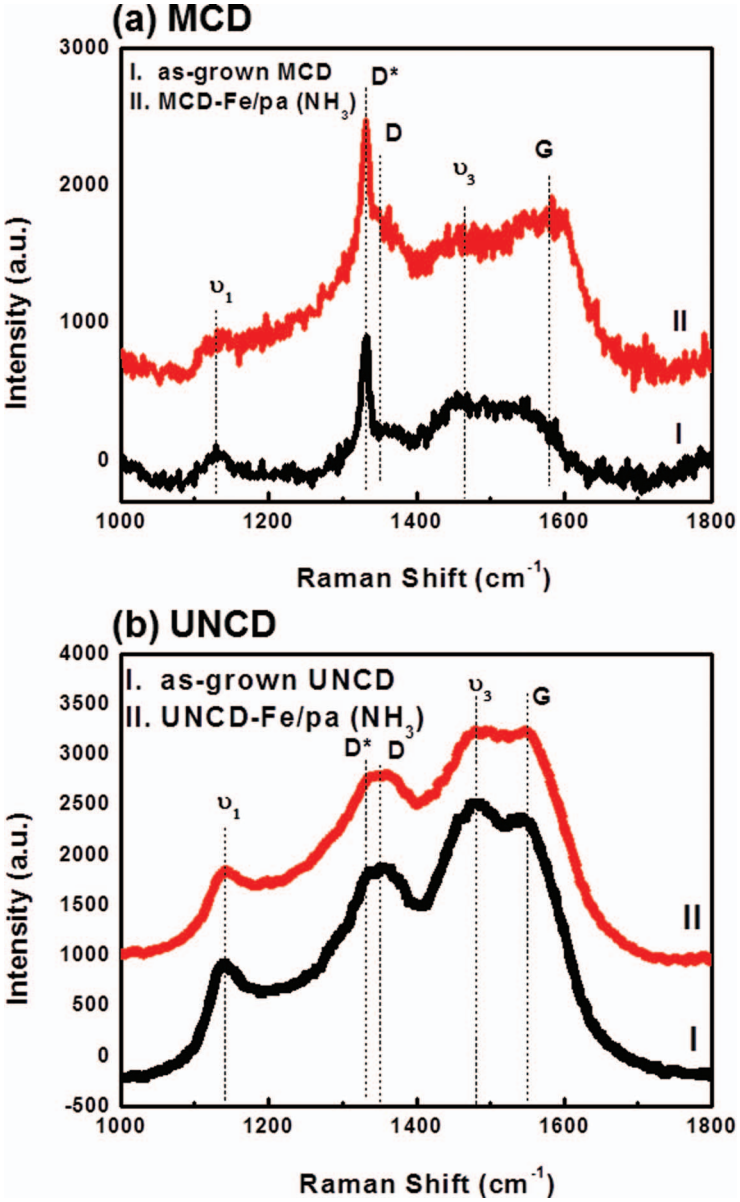

FIG. 2. The Raman spectroscopy of the (a) MCD films and (b) UNCD films, where the curves (I) are the as-grown films and the curves (II) are the Fe-coated/annealed ones.

sharp D-band resonance peak at 1332 cm^{-1} (curve I, Fig. 2(a)) along with small proportion of diffused resonance peaks at 1140 cm^{-1} (ν_1-band), 1480 cm^{-1} (ν_3-band), 1350 cm^{-1} (D^*-band) and 1580 cm^{-1} (G-band). The ν_1- and ν_3-band represent the trans-polyacetylene phase,[32,33] whereas the D^*- and G-band represent the disordered carbons,[34,35] along the grain boundaries. It should be noted that since the Raman spectroscopy at visible light (514.5 nm) is several times more sensitive to the sp^2-bonded carbons than to the sp^3-bonded ones, the presence of sp^2-bond related band in the Raman spectra does not imply that MCD films contain large proportion of sp^2-bonded carbons. In contrast, Raman spectra corresponding to UNCD films show prominent diffused ν_1-, ν_3- G*- and D*-band resonance peaks (curve I, Fig. 2(b)). No D-band resonance peak is observable. The invisibility of D-band resonance peak is, again, due to large fluorescence signal of visible light to the sp^2-bonded materials, that does not imply the absence of the sp^3-bonded species in the UNCD materials. These

All article content, except where otherwise noted, is licensed under a Creative Commons Attribution 3.0 Unported license. See: http://creativecommons.org/licenses/by/3.0/
Downloaded to IP: 163.13.36.187 On: Tue, 14 Apr 2015 07:05:07

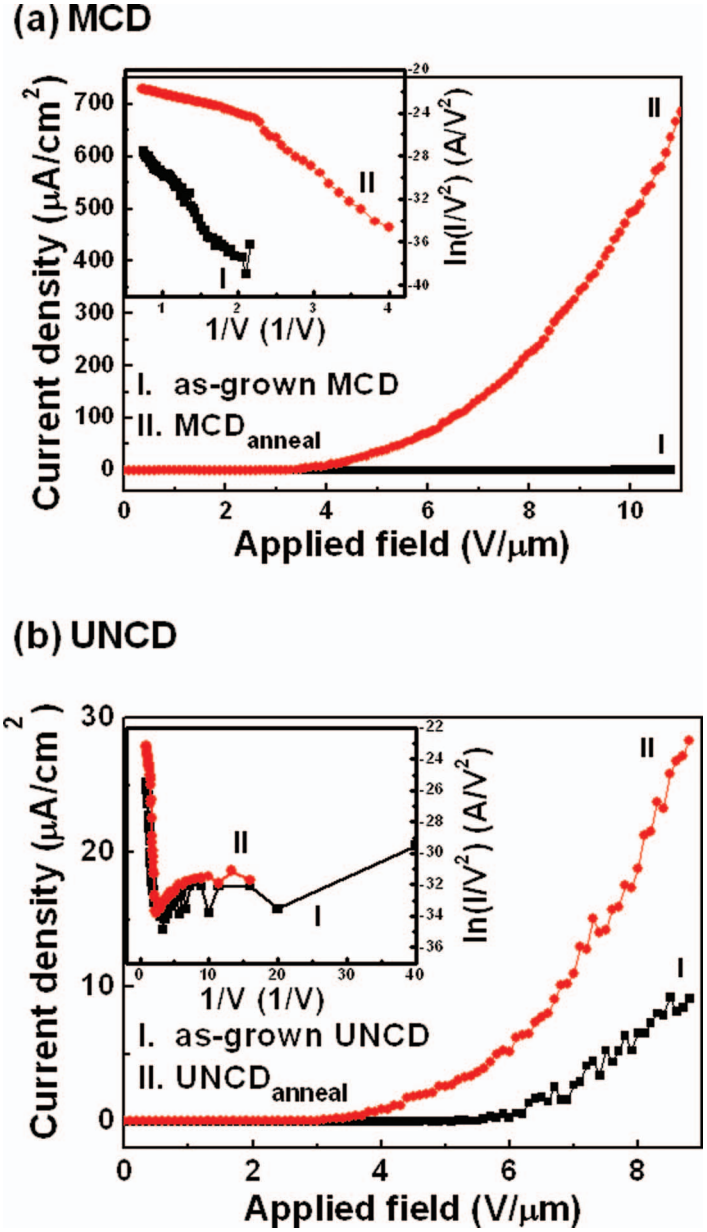

FIG. 3. The EFE properties of the (a) MCD films and (b) UNCD films, where the curves (I) are the as-grown films and the curves (II) are the Fe-coated/annealed ones.

Raman spectra are typical characteristics of diamond films with large and ultra-small grain granular structure, respectively.

The s-EFE properties of the as-deposited MCD and UNCD films are shown as curve I in Figs. 3(a) and 3(b), respectively. The turn-on field (E_0) and s-EFE current density (J_e) values were extracted from the J-E curves and were listed in Table I. The s-EFE process for the as-deposited MCD films can be turned on at $(E_0)_{MCD} = 9.9$ V/μm, attaining an EFE current density of $(J_e)_{MCD} = 1.9$ μA/cm^2 at an applied field of 8.8 V/μm (curve I, Fig. 3(a)), whereas the as-deposited UNCD films need only $(E_0)_{UNCD} = 3.3$ V/μm to turn on the s-EFE process, attaining larger s-EFE current density of $(J_e)_{UNCD} = 9.1$ μA/cm^2 at the same applied field (curve I, Fig. 3(b)). Figure 3 reveals that the MCD films required higher turn-on field than the UNCD films do to initiate the s-EFE process that is apparently due to the lower surface conductivity of the MCD films, as compared with that of

All article content, except where otherwise noted, is licensed under a Creative Commons Attribution 3.0 Unported license. See: http://creativecommons.org/licenses/by/3.0/
Downloaded to IP: 163.13.36.187 On: Tue, 14 Apr 2015 07:05:07

TABLE I. The surface electron field emission properties (s-EFE)[1] of the as-grown and Fe-coated/H_2-annealed diamond films.

materials	annealing temperature	E_0[2] (V/μm)	J_e[3] (μA/cm^2)
$MCD_{as\text{-}grown}$	-	9.9	1.9
$MCD_{Fe/pa}$	900°C	3.4	685.0
$UNCD_{as\text{-}grown}$	-	3.3	9.1
$UNCD_{Fe/pa}$	900°C	3.5	102.0

[1]s-EFE: the surface field emission properties measured by a parallel plate setup, in which the Cu-foil attached to the bottom of Si-substrate was wrapped over to contact the surface of the diamond films.
[2]E_0: the turn on field designated as the interception of the straight lines extrapolated from the high field and low field segments of the F-N plot.
[3]J_e: the EFE current density at an applied field of $E_a = 8.8$ V/μm.

the UNCD films. The s-EFE properties observed in Fig. 3 are markedly better than those commonly observed for the through film EFE properties for the MCD (or UNCD) films with turn-on field of >40 V/μm[5,36] and 10-12 V/μm,[17,18] respectively.

Moreover, Fig. 3 shows that, only the turn-on field (E_0) of MCD films was markedly lowered. But the s-EFE current density (J_e) for both the MCD and UNCD films was significantly increased due to Fe-coating/annealing processes. For the Fe-coated/annealed MCD films, the turn-on field for s-EFE process decreased to 3.4 V/μm, while the s-EFE current density at 8.8 V/μm increased to $(J_e)_{MCD} = 685.0$ μA/cm^2 (cf. Table I). In contrast, for the Fe-coated/annealed UNCD films, the turn-on field is about the same (3.5 V/μm), but the s-EFE current density (J_e) at 8.8 V/μm increased to $(J_e)_{UNCD} = 102.0$ μA/cm^2. The implication of these observations is that the Fe-coating/annealing processes induced a surface layer, which is much more conducting than the surface of MCD films but is only of comparable conductivity with the surface of UCND films.

Figure 4 shows the modification on the surface morphology of MCD and UNCD films resulted from the Fe-coating/annealing processes. There formed a network structure with some nano-particles (white color) sparsely distributed on the surface for both Fe-coated/annealed MCD and UNCD films, indicating the occurrence of rigorous Fe-to-diamond interaction. The network structure is denser for the MCD films (Fig. 4(a)), as compared with that for the UNCD films (Fig. 4(b)), implying that the Fe-clusters interacted with MCD films more markedly. Notably, the morphology of the films was not changed for the samples Fe-coated/annealed at a temperature lower than 800°C. Only small Fe-clusters, about a few nano-meters in size were formed (not shown), regardless of the nature of diamond films. The Fe-clusters started to interact with diamond films when the post-annealing temperature was increased to 900°C that markedly modified the surface morphology of the films. The extent of enhancement on the s-EFE properties is intimately related to the characteristics of network structure resulted from the Fe-coating/annealing processes. The Raman structure of the diamond films was not markedly altered due to the Fe-coating/annealing processes. Figure 2 indicates that the Raman spectra of MCD films are still predominated with sharp D-band (1332 cm^{-1}) resonance peak (curve II, Fig. 2(a)), whereas those of UNCD films are still predominated with diffused ν_1-, ν_3-, D*- and G-band resonance peaks (curve II, Fig. 2(b)). Detailed investigation reveals the occurrence of slight blue-shift for the Fe-coated/annealed processes diamond films. However, the Raman spectroscopy represents the structure of the whole diamond films and cannot provide clear information about how the Fe-coating/annealing processes modify the surface of the diamond films.

To understand the genuine factor that these processes enhanced the EFE properties of the MCD and UNCD films differently, the surface structure of these films need to be more detailed characterized using TEM. It should be noted that, for the purpose of preparing a thin foil contains mainly the materials near the surface region of the films, the samples were ion-milled from the Si side. The bright field (BF) image acquired in TEM mode for a typical region in MCD films is shown in Fig. 5(a), revealing that the these films consist of large diamond grains. The SAED shown as inset in this figure reveals that the diffraction spots are arranged in a ring shape, indicating that the large diamond grains in these materials are randomly oriented. In addition to the discrete diffraction

All article content, except where otherwise noted, is licensed under a Creative Commons Attribution 3.0 Unported license. See: http://creativecommons.org/licenses/by/3.0/
Downloaded to IP: 163.13.36.187 On: Tue, 14 Apr 2015 07:05:07

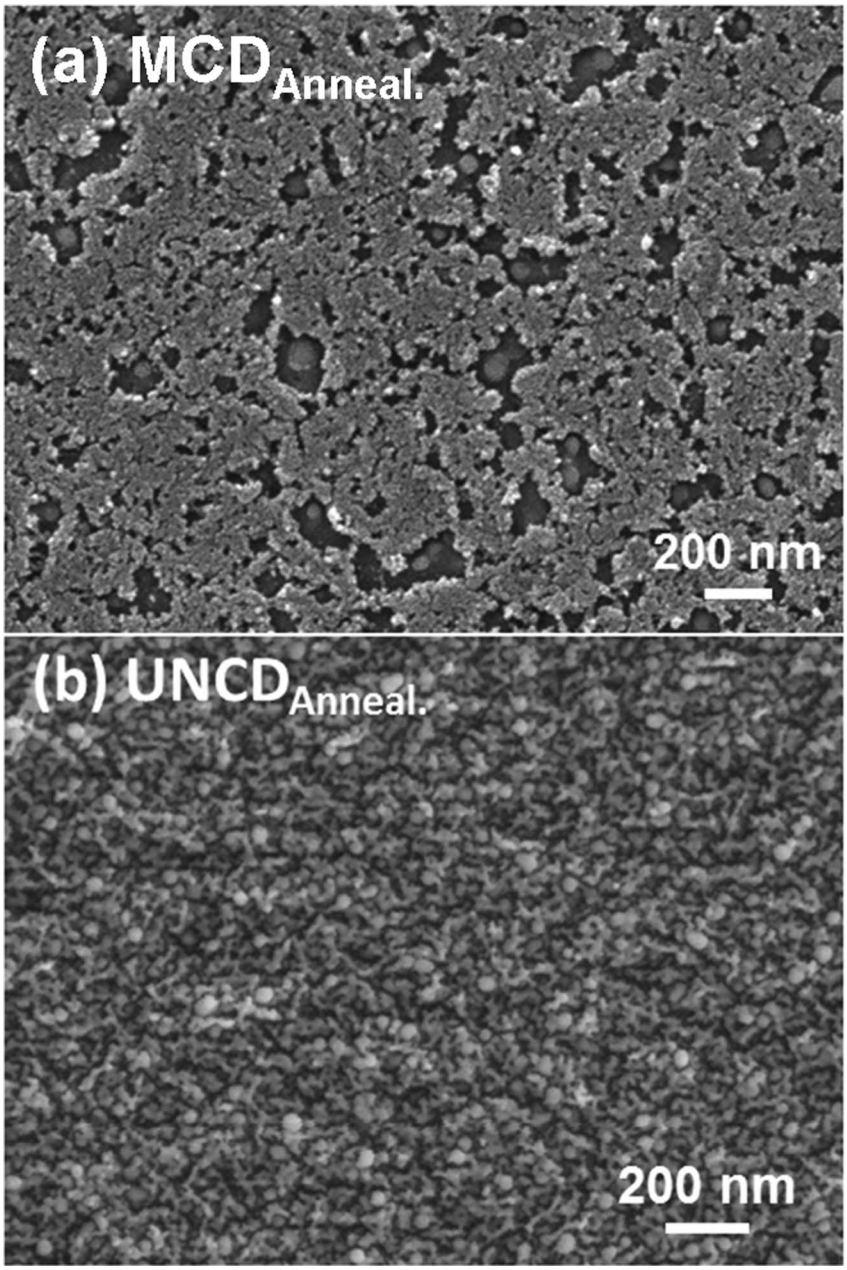

FIG. 4. The SEM micrograph of the Fe-coated/annealed (a) MCD films and (b) UNCD films.

spots, there appears a diffused diffraction ring in the center SAED, implying the existence of some amorphous (or graphitic) phase. Such a phenomenon will be more detailed analyzed shortly. The structure image of the area corresponding to region A in the BF image (cf. Fig. 5(a)) is shown in Fig. 5(b). The Fourier-transformed diffractogram image (F_{0b}) corresponding to the whole structure image in Fig. 5(b) contains streaks along 111 directions and systematic row of diffraction spots. The streaks correspond to the region with parallel fringes of irregular spacing, which are highlighted as area 1 and the FT-image (FT_1) in Fig. 5(b), are the planar defects, the stacking faults.[37] In contrast, the systematic row of diffraction spots corresponds to area 2 and FT_2, indicating that the region with parallel fringes of regular spacing contained in this area is the hexagonal diamond.[37] Moreover, the detailed microstructure of the peripheral region B, which is in adjacent to region A (cf. Fig. 5(a)), is shown in Figs. 5(c). There are abundant curved fringes (areas 5 in Fig. 5(c)), which were located

All article content, except where otherwise noted, is licensed under a Creative Commons Attribution 3.0 Unported license. See: http://creativecommons.org/licenses/by/3.0/
Downloaded to IP: 163.13.36.187 On: Tue, 14 Apr 2015 07:05:07

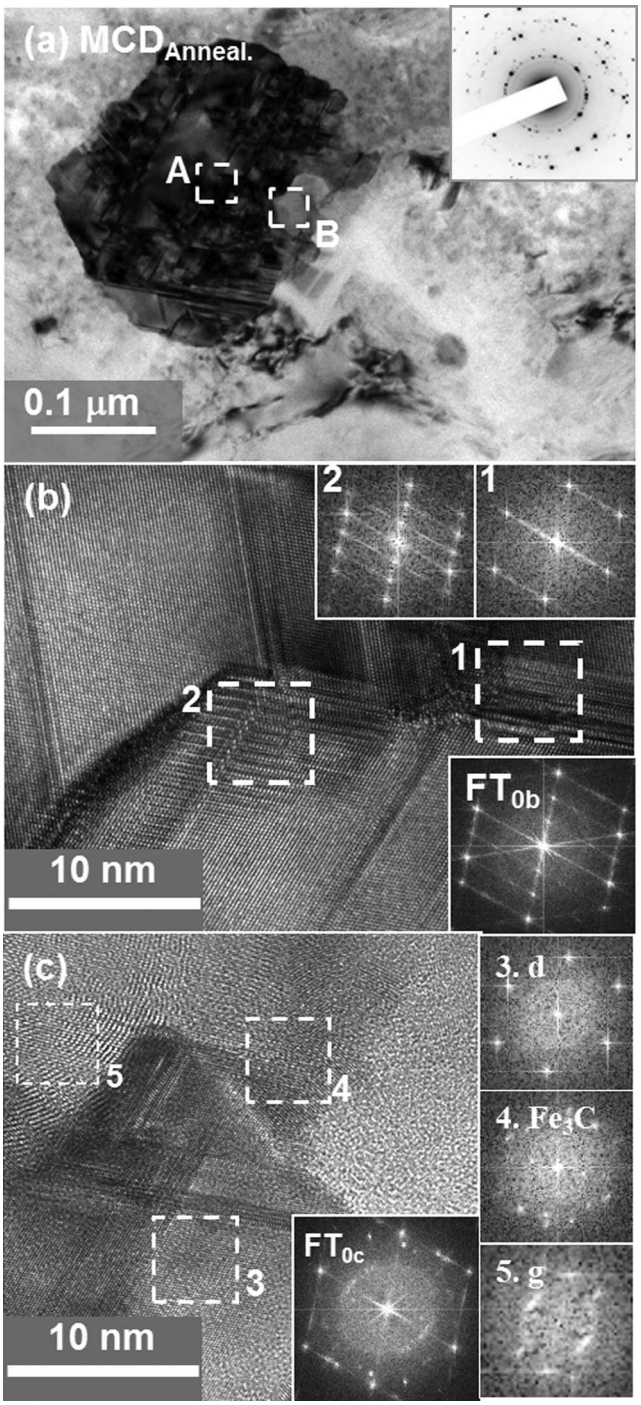

FIG. 5. The (a) TEM bright field image of the Fe-coated/annealed MCD films with the SAED shown as inset; (b, c) the TEM structure images corresponding to (b) the center of the diamond grains designated as A in "a" and (c) the peripheral region in adjacent to A, designated as B in "a".

in adjacent to the diamond (areas 3 in Fig. 5(c)). The FT image (FT_5) indicates that the curved fringes are of graphitic materials. The presence of the diamond was inferred by the FT image FT_3 in Fig. 5(c). In between the diamond and graphitic phase, there exists a second phase (area 4) about tens of nanometer in thickness, which is Fe_3C phase, as indicated by the FT image (FT_4). The implication of these observations is that the Fe-clusters interacted with the diamond rigorously at annealing process, dissolved the carbons and re-precipitated them at the other side of Fe-clusters to

All article content, except where otherwise noted, is licensed under a Creative Commons Attribution 3.0 Unported license. See: http://creativecommons.org/licenses/by/3.0/
Downloaded to IP: 163.13.36.187 On: Tue, 14 Apr 2015 07:05:07

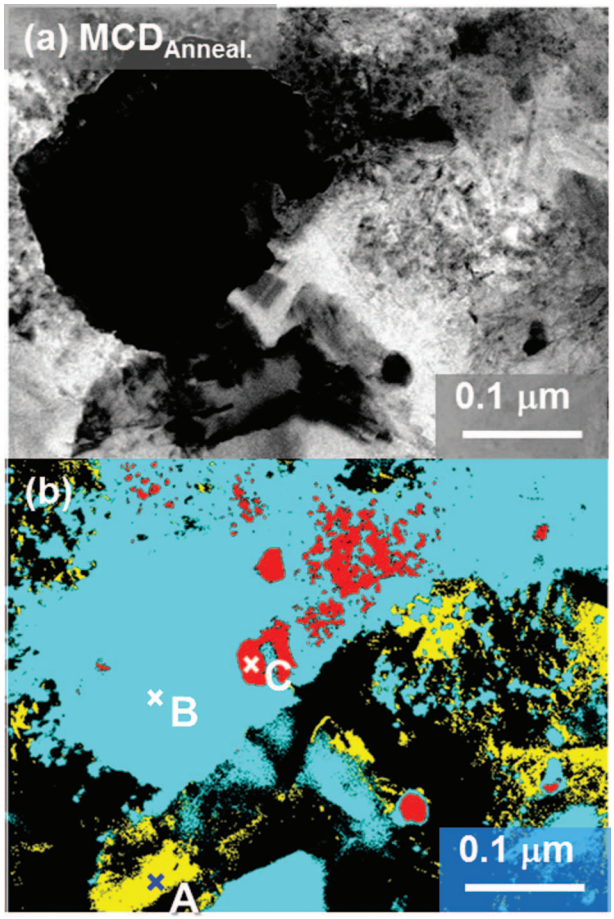

FIG. 6. The (a) STEM bright field, BF, image and (b) high angle annular dark field, HAADF, images for the Fe-coated/annealed MCD films of the same region as that shown in Fig. 5(a).

form nano-sized graphite clusters. Such an interaction is similar with the growth of carbon nanotubes via the Fe-catalysts.[38–41] Presumably, the Fe_3C clusters were formed when the samples were cooled fastly that frozen the un-precipitated carbons in the clusters.

However, the TEM bright field image cannot elucidate the distribution of different species contained in the films. It required HAADF image to clearly resolve them. Figure 6(a) shows the typical bright field (BF) image acquired under scanning transmission electro microscopic (STEM) mode for the same region in Fe-coated/annealed MCD films as those shown in Fig. 5(a). The STEM image cannot shows the microstructure of the materials as detail as the BF image in TEM mode, but it can reveal the element distribution of more clearly. Notably, for the Fe-coated/annealed MCD films shown in Fig. 6(a), only iron and carbon (diamond, graphite or amorphous carbon) species are involved. The contribution of the two species can be clearly resolved by systematically changing the camera length (CL), and hence the scattering angle (α), in acquiring the HAADF signals. Figure 6(b) illustrates a typical composed-HAADF image, which is superposition of the HAADF images acquired with $\alpha_1 = 35$ mrad (yellow color), $\alpha_2 = 110\sim300$ mrad (blue color) and $\alpha_3 = 150\sim400$ mrad (red color). To further identify the species contained in different regions, the typical EDAX (in STEM mode) patterns corresponding to the yellow, blue and red regions, which were designated as A, B and C in Fig. 6(b), were acquired and were plotted as profiles I, II and III in Fig. 7, respectively. These EDAX patterns clearly indicate that the profile I, which corresponds to location A, contains mostly the carbon, whereas the EDAX profile III, which corresponds to location C, contains mainly large Fe-signals. These profiles indicate that the yellow-colored region is the carbon (diamond, amorphous carbon or graphite), whereas the red-colored region is the Fe-clusters. The EDAX profile

All article content, except where otherwise noted, is licensed under a Creative Commons Attribution 3.0 Unported license. See: http://creativecommons.org/licenses/by/3.0/
Downloaded to IP: 163.13.36.187 On: Tue, 14 Apr 2015 07:05:07

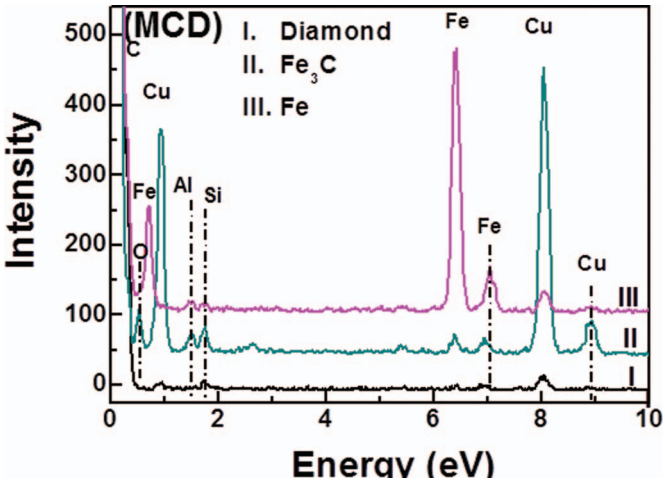

FIG. 7. The EDAX (STEM) profiles for the Fe-coated/annealed MCD films. The spectra I, II and III correspond to the locations A, B, and C designated in Fig. 6(b).

II corresponding to location B contains both Fe and C signals, implying this blue-colored region might be the compound of Fe and C, most probably, the Fe_3C-clusters. The small signals are Cu, Au and Si, which are presumably the contaminations induced in the ion-milling process from the underlying substrates and the Cu-mesh. These results indicate that HAADF technique can resolved very well the distribution of the species in diamond films.

The powerfulness of HAADF technique for identifying the distribution of species in Fe-coated/annealed MCD films is further demonstrated by the 3D-tomoraphy in TEM. Notably, in the construction of the 3D tomography, only the HAADF images correspond to Fe_3C ($\alpha_2 = 110$ mrad) and Fe ($\alpha_3 = 150$ mrad) were superimposed. The HAADF images corresponding to diamond ($\alpha_1 = 35$ mrad) cannot be used for constructing the 3D tomography, since the contrast of the crystalline diamond materials fluctuate largely when the samples were tilted through a zone axis. Therefore, only the distribution of the Fe and Fe_3C clusters near the grain boundary region of the diamond grains are observable. Those on the surface of the diamond grain cannot be successfully acquired. The video showing the 3D-tomography of the Fe-coated/annealed MCD films was shown as supplementary information (Fig. 8). Viewing the 3D-tomography from different angles by rotating the 3D-tomography reveals that (i) the Fe and Fe_3C clusters are mainly located at the surface of the diamond grains, which is expected as the clusters were formed by the Fe-to-diamond interaction, and (ii) the Fe_3C-clusters (white colored) are interconnected forming a continuous network and the Fe-clusters (red colored) are located on top of the Fe_3C-clusters in a form of isolated particulates. Such information can be obtained only through the reconstruction of the distribution of species in 3 dimensional manners, the 3D-tomography. Figure 8(a) shows a stereographic projection of the 3D-tomography, whereas Figs. 8(b) and 8(c) show the X-Y and Y-Z projection of the 3D-tomography. These observations imply, again, that The Fe_3C clusters are resulted by Fe-to-diamond interaction and the Fe-clusters are the un-reacted Fe-coating. The X-Y projection of the 3D-tomography (Fig. 8(b)) more faithfully revealed the distribution of the Fe- and Fe_3C-clusters, as compared with the simple HAADF image (cf. Fig. 6(b)). Only via the 3D-tomography can the phenomenon that the F_3C-cluster network was located underneath the Fe-cluster one be unambiguously resolved.

The above-mentioned TEM investigations revealed that the formation of nano-graphite clusters due to Fe-to-diamond interaction is the authentic factor that enhanced the s-EFE properties of the Fe-coated/annealed MCD films. However, it is still not explained why the same heat-treatment process applied to UNCD films cannot lead to the same beneficial effect on improving their s-EFE properties. To understand how the Fe-coating/annealing processes influences the evolution of the microstructure of the MCD and UNCD films in different manners, the surface microstructure of the UNCD films was also investigated using HAADF and 3D-tomography techniques. Figures 9(a) shows typical

All article content, except where otherwise noted, is licensed under a Creative Commons Attribution 3.0 Unported license. See: http://creativecommons.org/licenses/by/3.0/
Downloaded to IP: 163.13.36.187 On: Tue, 14 Apr 2015 07:05:07

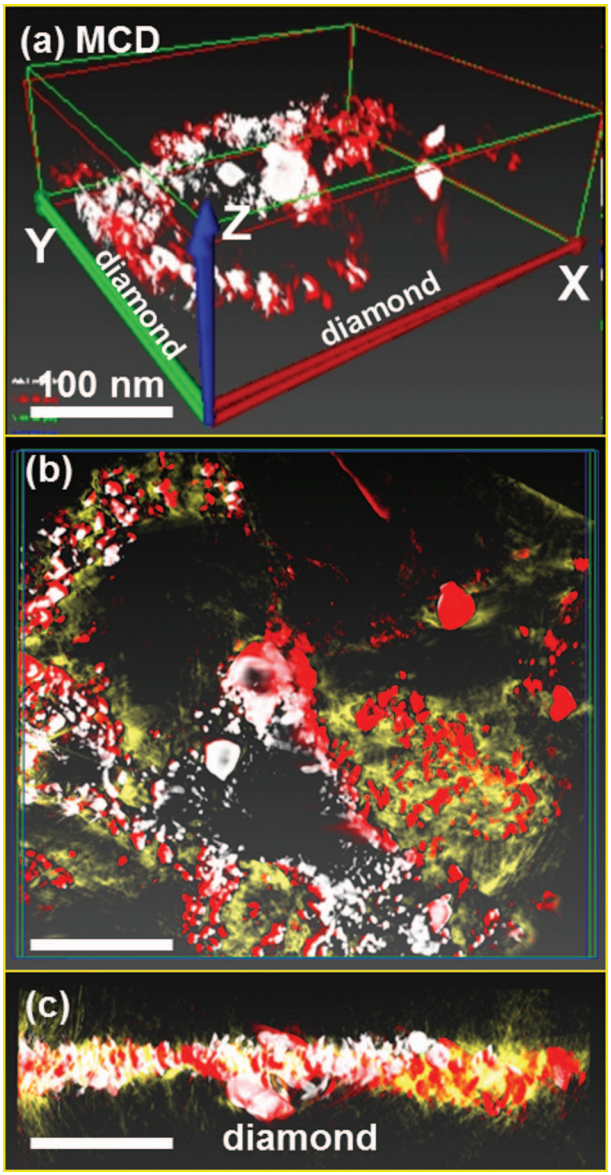

FIG. 8. The video of the TEM 3D-tomography of the Fe-coated/annealed MCD films, showing the distribution of Fe- and Fe_3C-clusters on these films. The two-component 3D-tomography for the Fe-coated/annealed MCD films: (a) stereographic projection, (b) X-Y projection and (c) Y-Z projection of the tomography. The Fe-clusters are in red color and the Fe_3C-clustes are in white color (the bar in "b" and "c" is 100 nm) (enhanced online) [URL: http://dx.doi.org/10.1063/1.4748865.1] .

TEM BF image for the Fe-coated/annealed UNCD films with the inset showing the corresponding SAED. The diffraction spots are arranged in a smooth ring, implying that this region mainly contain ultra-small randomly oriented diamond grains. Figure 9(b) shows the STEM BF image of the same region that shows, again, the BF(STEM) micrographs cannot resolve the microstructure in the same detail manners as the BF(TEM) micrographs do. Figure 9(c) illustrates a corresponding composed-HAADF image, which is superposition of the HAADF images acquired with $\alpha_1 = 35$ mrad (yellow color), $\alpha_2 = 110$ mrad (blue color) and $\alpha_3 = 150$ mrad (red color). The EDAX (in STEM mode) patterns corresponding to the regions A (yellow color), B (blue color) and C (red color) designated in Fig. 9(c) were plotted as profiles I, II and III in Fig. 10, respectively. These EDAX patterns clearly indicate that the location A (profile I) contains mostly the carbon, the location B (profile II) contains

All article content, except where otherwise noted, is licensed under a Creative Commons Attribution 3.0 Unported license. See: http://creativecommons.org/licenses/by/3.0/
Downloaded to IP: 163.13.36.187 On: Tue, 14 Apr 2015 07:05:07

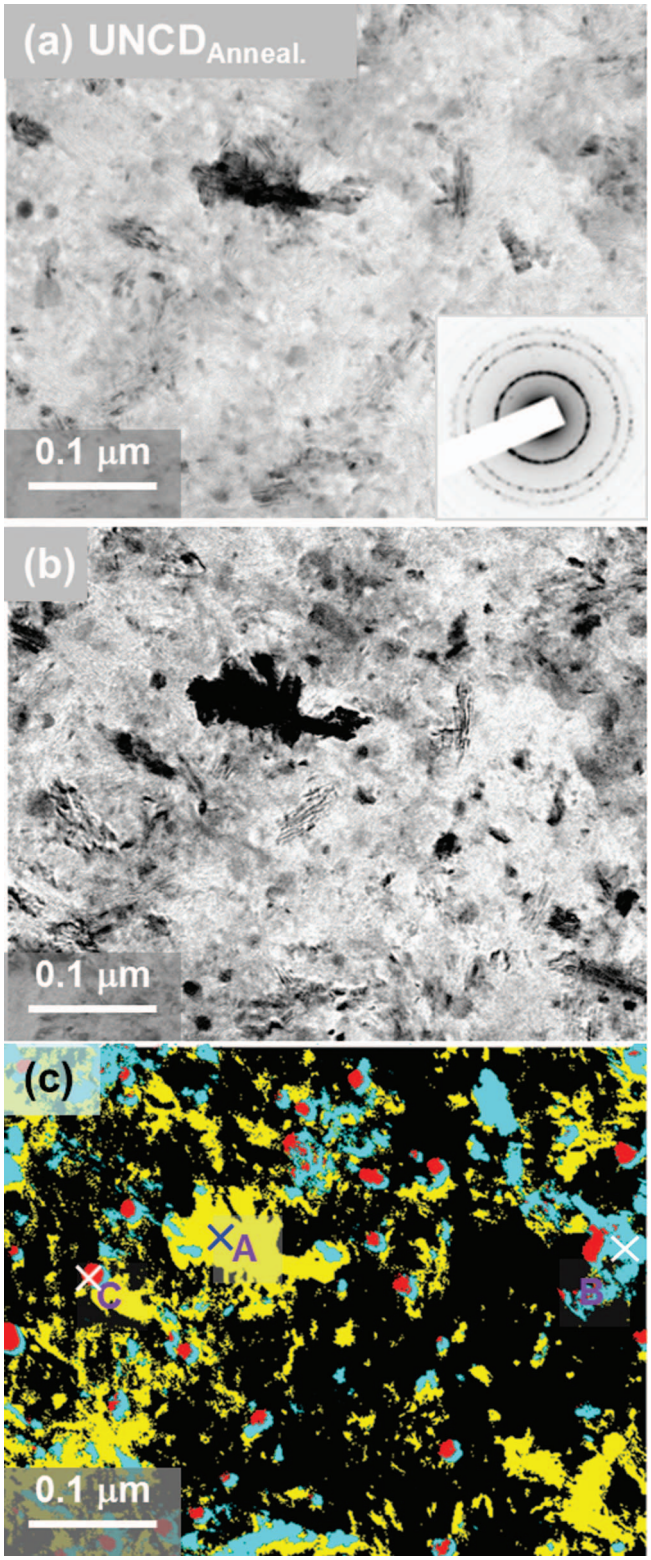

FIG. 9. The (a) TEM bright field, BF, (b) STEM bright field, BF, and (c) high angle annular dark field, HAADF, images for the Fe-coated/annealed UNCD films.

All article content, except where otherwise noted, is licensed under a Creative Commons Attribution 3.0 Unported license. See: http://creativecommons.org/licenses/by/3.0/
Downloaded to IP: 163.13.36.187 On: Tue, 14 Apr 2015 07:05:07

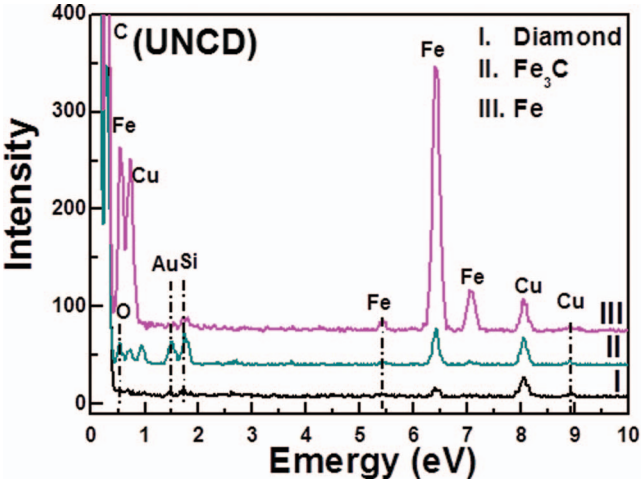

FIG. 10. The EDAX (STEM) profiles for the Fe-coated/annealed UNCD films. The spectra I, II and III correspond to the locations A, B, and C designated in Fig. 9(c).

the Fe_3C clusters and the location C (profile III) contains the Fe-clusters. Again, the small signals of Cu, Au and Si are the contaminations from the underlying substrates and the Cu-mesh.

The 3D tomography was, again, constructed from the HAADF images taken at different tilting of the samples ($+70^\circ$ to -70°, 2° each step) to more clearly illustrate the distribution of the Fe- and Fe_3C-clusters in these films. Figure 11(a) shows the stereographic projection of the 3D tomography of the Fe-coated/annealed UNCD films, whereas the Figs. 11(b) and 11(c) are the X-Y and Y-Z projections of the 3D tomography (the video for the 3D tomography of the Fe-coated/annealed UNCD films is shown as supplementary information Fig. 11). These figures illustrate that the Fe-clusters (red color) and Fe_3C-clusters (white color) are mainly located on the surface of the diamond films for the Fe-coated/annealed UNCD films. The Fe-clusters and Fe_3C-clusters are distributed evenly on the surface of diamond films. To reveal the distribution of the nanographite clusters, the carbon signal in HAADF was included in the 3D-tomography. Figure 12(a) shows the stereographic projection, whereas Fig. 12(b) and 12(c) show the X-Y and Y-Z projections of the carbon containing 3D-tomography, respectively. These figures illustrate that the nanographitic clusters are distributed among the Fe- and Fe_3C-clusters. The nanographitic clusters covered the surface of UNCD films, that is evidently the authentic factor that the Fe-coating/annealing processes enhanced the s-EFE properties for the UNCD films. The 3D tomography observations are in accord with the arguments that Fe-clusters interacted with the diamond and catalytically induced the formation of nano-graphitic clusters in the Fe-coating/annealing processes. The intriguing observation is that the Fe- and Fe_3C-clusters were distributed on the UNCD surface in a totally different manners from that on the MCD films. The Fe- and Fe_3C-clusters are mixing together for UNCD films, rather than formed sequentially one on top of the other as that for MCD films. Such an observation implies that, while some of the Fe-clusters reacted with diamond to form Fe_3C-cllusters, some of them remain unreacted. It is believed that the nano-graphites were induced in accompanied with the formation of Fe_3C-cllusters and the distribution of nano-graphites is closely associated with that of the Fe_3C-cllusters. Therefore, Fig. 12 implies that the nano-graphites formed on UNCD surface do not completely interconnected and, thereafter, is less effective in enhancing the s-EFE properties for UNCD films. Such information can only be conceived by viewing the 3D-tomography from different angles.

IV. DISCUSSION

The Fe-coating/annealing process can efficiently induce the formation of nano-graphite phase via the Fe-to-diamond interaction, regardless of whether the diamond films are MCD or UNCD. However, detailed analysis on the 3-D tomography revealed a subtle difference in the distribution

All article content, except where otherwise noted, is licensed under a Creative Commons Attribution 3.0 Unported license. See: http://creativecommons.org/licenses/by/3.0/
Downloaded to IP: 163.13.36.187 On: Tue, 14 Apr 2015 07:05:07

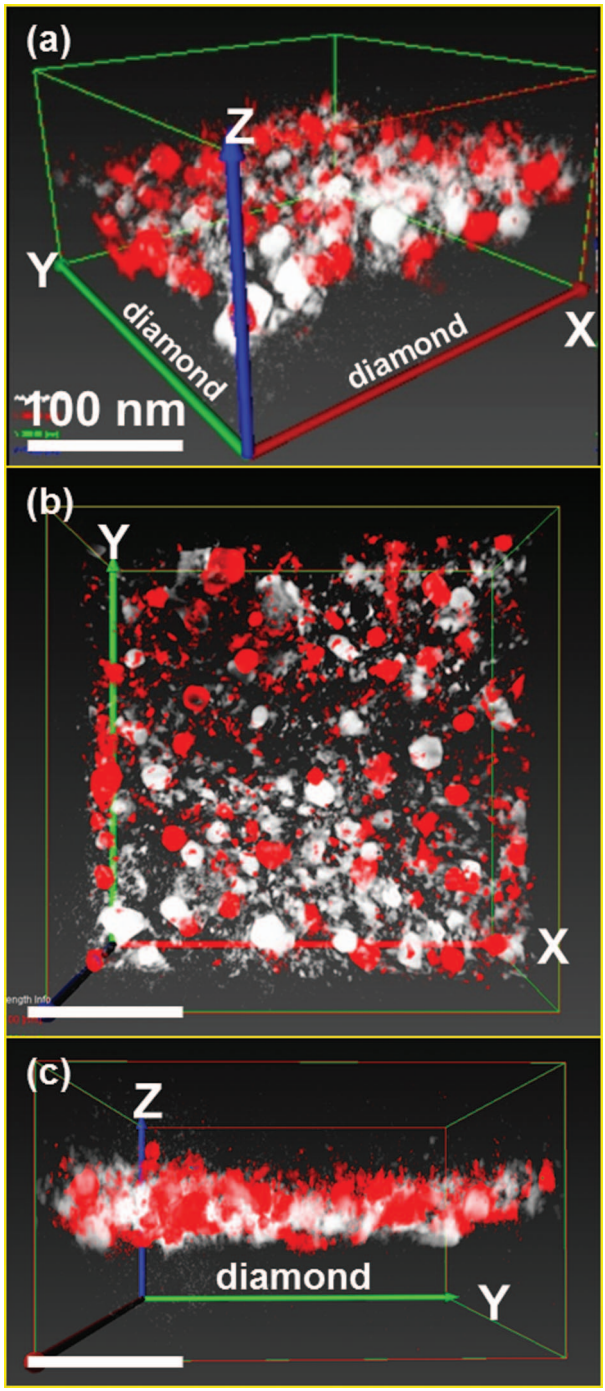

FIG. 11. The video of the TEM 3D-tomography of the Fe-coated/annealed UNCD films, showing the distribution of Fe-, Fe_3C- and nanographite clusters on these films. The two-component 3D-tomography for the Fe-coated/annealed UNCD films: (a) stereographic projection, (b) X-Y projection and (c) Y-Z projection of the tomography. The Fe-clusters are in red color and the Fe_3C-clustes are in white color (the bar in "b" and "c" is 100 nm) (enhanced online) [URL: http://dx.doi.org/10.1063/1.4748865.2] .

All article content, except where otherwise noted, is licensed under a Creative Commons Attribution 3.0 Unported license. See: http://creativecommons.org/licenses/by/3.0/
Downloaded to IP: 163.13.36.187 On: Tue, 14 Apr 2015 07:05:07

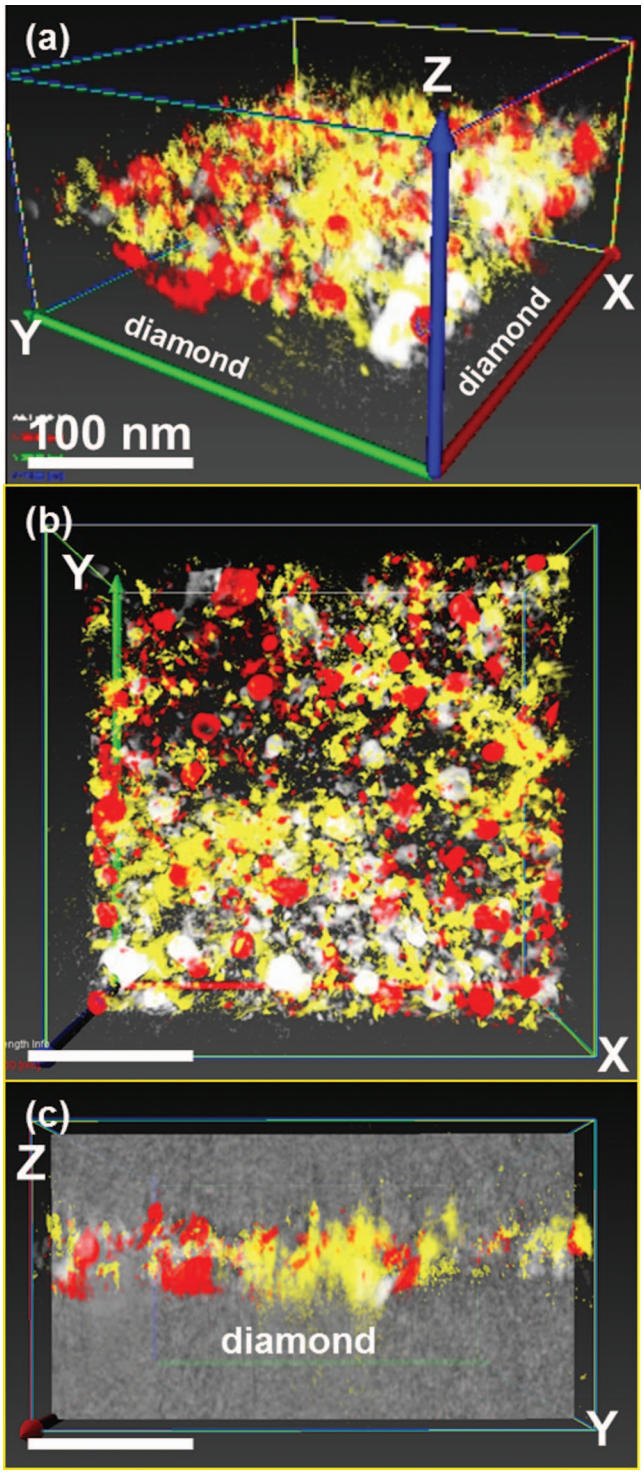

FIG. 12. The video of the TEM 3D-tomography of the Fe-coated/annealed UNCD films, showing the distribution of Fe-, Fe_3C- and nanographite clusters on these films. The three-component 3D-tomography for the Fe-coated/annealed UNCD films: (a) stereographic projection, (b) X-Y projection and (c) Y-Z projection of the tomography. The Fe-clusters are in red color, the Fe_3C-clustes are in white color and the nano-graphitic-clusters are in yellow color (the bar in "b" and "c" is 100 nm). (see Fig. 11 for video)

All article content, except where otherwise noted, is licensed under a Creative Commons Attribution 3.0 Unported license. See: http://creativecommons.org/licenses/by/3.0/
Downloaded to IP: 163.13.36.187 On: Tue, 14 Apr 2015 07:05:07

of the Fe and Fe_3C nano-clusters. For MCD films, the Fe_3C-clusters always formed underneath the Fe-clusters, located in between the Fe-clusters and the diamond surfaces, whereas, for UNCD films, the Fe_3C-clusters were distributed among the Fe-clusters as independent particles. The difference in morphology of these clusters formed on the Fe-coated/annealed MCD and UNCD films is closely related with the different granular structure of the two diamond films. For MCD films, the grains are large (∼300 -500 nm) and the surface are clean. The surface terminations, hydrogen or oxygen, can be easily removed during the DC sputtering process for coating the Fe layer. The Fe-clusters are directly in contact with the diamond surface. The Fe-to-diamond interaction readily occurred and most of the Fe-clusters catalytically dissociated the diamond lattices simultaneously when the annealing temperature reached 900°C, resulting in a continuous Fe_3C layer beneath the Fe-clusters. It is expected that there are nanographitic-clusters formed, associating with each of the Fe_3C-clusters. The nano-graphite-clusters thus formed a continuous network, which facilitated the transportation of electrons and markedly enhanced the surface EFE process. In contrast, for the UNCD films, the size of the diamond grains is extremely small (∼5 nm). The grain boundaries and, presumably, the surface of the UNCD films were covered with a thin layer of hydrocarbon (e.g. trans-polyacetylene). The Fe-clusters do not directly in contact with the diamond. Only some of the Fe-clusters can dissociate the hydrocarbon layer, triggering the Fe-to-diamond interaction and inducing the formation of nanographite clusters. Some of them remained unreacted. The Fe_3C-clusters are mostly isolated from one another. The nano-graphitic clusters, whose morphology is intimated associated with the distribution of Fe_3C-clusters, are not well interconnected.

Restated, although the Fe-to-diamond interaction will be induced in the Fe-coating/annealing processed, the distribution of the resulted nano-clusters differs markedly for the MCD and UNCD films that is closely related to the different granular structure of these films. The F_3C clusters are located underneath the Fe-clusters, forming a continuous layer for the MCD films, but are distributed among the Fe-clusters as isolated clusters for the UNCD films. Therefore, the nano-graphite clusters, whose distribution is intimately correlated with that of the Fe_3C-clusters, formed an interconnected network for MCD films that facilitated the electron transport and enhanced the s-EFE process more markedly. In contrast, the nano-graphitic clusters formed on the surface of the UNCD films are isolated. The s-EFE process is thus only moderated improved for these films. The understanding on the distribution of nano-clusters is of prime importance in elucidating the authentic factor that influences the s-EFE behavior of the diamond. Such an understanding is possible only through the 3D-tomographic investigation of the materials.

V. CONCLUSION

When the MCD or UNCD films were coated with a thin Fe-layer (∼10 nm) and annealed in reduced atmosphere at 900°C for 5 min, the surface of the diamond films became very conductive and exhibited enhanced surface electron field emission (s-EFE) properties, regardless of the nature of the diamond films. The Fe-coating/annealing processes improved the s-EFE properties for the MCD films more markedly than that for the UNCD films. While it is evident that the enhancement in s-EFE properties is owing to the formation of nano-graphite clusters via the Fe-to-diamond interaction, the morphology of the clusters thus formed varied with the granular structure of the diamond films. The TEM 3D-tomographic investigation shows that the Fe-, Fe_3C and nano-graphitic clusters are all formed on the surface of the diamond films. The F_3C clusters are located underneath the Fe-clusters, forming a continuous layer for the MCD films, but are distributed among the Fe-clusters as isolated clusters for the UNCD films. The morphology of the nano-graphite clusters is intimately correlated with that of the Fe_3C-clusters. The nano-graphite clusters formed an interconnected network for MCD films that facilitated the electron transport and enhanced the s-EFE process more markedly, whereas the nano-graphitic clusters are isolated from one another on the surface of the UNCD films. The s-EFE process of the Fe-coated/annealed MCD films was markedly enhanced, i.e., it be turned on at $(E_0)_{MCD} = 3.4$ V/μm, achieving a large s-EFE current density of $(J_e)_{MCD} = 685.0$ μA/cm^2 at an applied field of 8.8 V/μm, as compared with $(E_0)_{UNCD} = 3.5$ V/μm and $(J_e)_{MCD} = 102.0$ μA/cm^2 at an applied field of 8.8 V/μm. Such kind of the detailed interaction between Fe and diamond can be elucidated only by 3D-tomographic investigations.

All article content, except where otherwise noted, is licensed under a Creative Commons Attribution 3.0 Unported license. See: http://creativecommons.org/licenses/by/3.0/
Downloaded to IP: 163.13.36.187 On: Tue, 14 Apr 2015 07:05:07

ACKNOWLEDGMENTS

The authors would like to thank the National Science Council, Republic of China for the support of this research through the Project Nos. NSC 99-2119-M-032- 003-MY2 and NSC100-2113-M -007-006.

[1] J. E. Field, *The Properties of Diamonds* (Academic, London, 1979).
[2] H. Liu and D. S. Dandy, Diamond Relat. Mater. **4**, 1173 (1995).
[3] J. C. Angus, H. A. Will, and W. S. Stanko, J. Appl. Phys. **39**, 2915 (1968).
[4] B. V. Spitsyn, L. L. Bouilov, and B. V. Derjaguin, J. Cryst. Growth **52**, 219 (1981).
[5] F. J. Himpsel, J. A. Knapp, J. A. Van Vechten, and D. E. Eastman, Phys. Rev. B **20**,624 (1979).
[6] V. S. Vavilov, Phys. Status Solidi A **31**, 11 (1975).
[7] K. Okano, H. Naruki, Y. Akiba, T. Kurosu, M. Iida, and Y. Hirose, Jpn. J. Appl. Phys. **27**, 173 (1988).
[8] P. Wurzinger, P. Pongratz, P. Hartmann, R. Haubner, and B. Lux, Diam. Relate. Mater. **6**, 763 (1997).
[9] T. Saito, M. Kameta, K. Kusakabe, S. Morooka, H. Maeda, Y. Hayashi, and T. Asano, Japn. J. Appl. Phys. **37**, L543 (1998).
[10] Satoshi Koizumi, Tokuyuki Teraji, and Hisao Kanda, Diam. Relat. Mater. **9**, 935 (2000).
[11] H. Kanda, K. W atanabe, S. Koizumia, and T. Teraji, Diam. Relate. Mater. **12**, 20 (2003).
[12] X. J. Hu, J. S. Ye, H. Hu, X. H. Chen, and Y. G. Shen, Appl. Phys. Lett. **99**, 131902 (2011).
[13] L. G. Wang and Alex Zunger, Phys. Rev. B **66**, 161202 (2002).
[14] Sakaguchi, M. N. Gamo, Y. Kikuchi, E. Yasu, H. Haneda, T. Suzuki, and T. Ando, Phys. Rev. B **60**, R2139 (1999).
[15] J. R. Petherbridge, P. W. May, G. M. Fuge, G. F. Robertson, K. N. Rosser, and M. N. R. Ashfold, J. Appl. Phys. **91**, 3605 (2002).
[16] G. Morell, A. Gonzalez-Berrıos, B. R. Weiner, and S. Gupta, J. Mater. Sci.: Mater. Electron **17**, 443 (2006).
[17] R. Krauss, O. Auciello, M. Q. Ding, D. M. Gruen, Y. Huang, V. V. Zhirnov, E. I. Givargizov, A. Breskin, R. Chechen, E. Shefer, V. Konov, S. Pimenov, A. Karabutov, A. Rakhimov, and N. SuetinL, J. Appl. Phys. **89**, 2598 (2001).
[18] T. D. Corrigan, D. M. Gruen, A. R. Krauss, P. Zapoa, and R. P. H. Chang; Diam. Rel. Mater. **11**(1), 43–48 (2002).
[19] S. Bhattacharyya, O. Auciello, J. Birrell, J. A. Carlisle, L. A. Curtiss, A. N. Goyette, D. M. Gruen, A. R. Krauss, J. Schlueter, A. Sumant, and P. Zapol, Appl. Phys. Lett. **79**(10), 1441–1443 (2001).
[20] D. Zhou, A. R. Krauss, L. C. Qin, T. G. McCauley, D. M. Gruen, T. D. Corrigan, R. P. H. Chan, and H. Gnaser, J. Appl. Phys. **82**, 4546 (1997).
[21] J. Birrell, J. E. Gerbi, O. Auciello, J. M. Gibson, D. M. Gruen, and J. A. Carlisle, J. Appl. Phys. **93**, 5606 (2003).
[22] Y. C. Chen, N. H. Tai, and I. N. Lin, Diam. Relate. Mater. **17**, 457 (2008).
[23] K. J. Sankaran, P. T. Joseph, N. H. Tai, and I. N. Lin, Diam. Relate. Mater. **19**, 927 (2010).
[24] C. R. Lin, W. H. Liao, D. H. Wei, J. S. Tsai, C. K. Chang, and W. C. Fang, Diam. Relate. Mater. **20**, 380 (2011).
[25] P. C. Huang, W. C. Shih, H. C. Chen, and I. N. Lin, J. Appl. Phys. **109**, 084309 (2011).
[26] K. Y. Teng, W. C. Shih, P. C. Huang, H. C. Chen, C. Y. Tang, and I. N. Lin, J. Appl. Phys., in press.
[27] R. H. Fowler and L. Nordheim, Proc. R. Soc. London, Ser. A **119**, 173 (1928).
[28] M. Weyland, Topics in Catalysis **21**(4), 175 (2002).
[29] P. A. Midgley, M. Weyland, Ultramicroscopy **96**, 413–431 (2003).
[30] S. Bals, G. Van Tendeloo, and C. Kisielowski, Adv. Mater. **18**, 892–895 (2006).
[31] http://www.jeolusa.com/RESOURCES/ElectronOptics/DocumentsDownloads/tabid/320/Default.aspx?EntryId=800.
[32] Z. Sun, J. R. Shi, B. K. Tay, and S. P. Lau, Diam. Relat. Mater. **9**, 1979 (2000).
[33] C. Ferrari and J. Robertson, Phys. Rev. B **63**, 121405 (2001).
[34] C. Ferrari and J. Robertson, Phys. Rev. B **61**, 14095 (2000).
[35] J. Michler, Y. von Kaenel, J. Stiegler, and E. Blank, J. Appl. Phys. **83**, 187 (1998).
[36] Y. C. Lee, S. J. Lin, I. N. Lin, and H. F. Cheng, J. Appl. Phys. **97**(5), 054310 (2005).
[37] I. N. Lin, H. C. Chen, C. S. Wang, Y. R. Lee, and C. Y. Lee, Cryst Eng Comm. **13**, 6082–6089 (2011).
[38] D. C. Li, L. Dai, S. Huang, A. W. H. Mau, and Z. L. Wang, Chem. Phys. Lett. **316**, 349 (2000).
[39] E. F. Kukovitsky, S. G. L'vov, and N. A. Sainov, Chem. Phys. Lett. **317**, 65 (2000).
[40] S. B. Sinnott, R. Andrews, D. Qian, A. M. Rao, Z. Mao, E. C. Dickey, and F. Derbyshire, Chem. Phys. Lett. **315**, 25 (1999).
[41] Gorbunov, O. Jost, W. Pompe, and A. Graff, Carbon **40**, 113 (2002).

All article content, except where otherwise noted, is licensed under a Creative Commons Attribution 3.0 Unported license. See: http://creativecommons.org/licenses/by/3.0/
Downloaded to IP: 163.13.36.187 On: Tue, 14 Apr 2015 07:05:07